

Amino Acid Composition and Wavelength Effects in Matrix-assisted Laser Desorption/Ionization

Zohra Olumee, Mehrnoosh Sadeghi, Xiaodong Tang, and Akos Vertes*

Department of Chemistry, The George Washington University, Washington, DC 20052, USA

SPONSOR REFEREE: Professor M. V. Johnston, University of Delaware, Newark, NJ 19716, USA

Ion yields were investigated in matrix-assisted laser desorption/ionization (MALDI) as a function of amino acid composition using a variable wavelength ion source. In the case of nitrogen laser excitation (337 nm), $[M + H]^+$ ions were abundant for short peptides containing basic or polar amino acid residues. The lack of basic residues led to diminishing ion formation at 337 nm. Increasing the chain length led to enhanced ionization even for peptides with non-polar side chains. In contrast to the liquid phase basicities the basic residues showed Arg > His > Lys order in their affinity to protons. Variations in the average ion yield showed decreasing trend with increasing basicity of the residues pointing to potential differences in the matrix incorporation of different guest molecules. Dye laser excitation at 280 nm resulted in extensive fragmentation and enhanced ion formation from peptides containing aromatic side chains indicating the possible role of analyte excited states in ion formation. Semi-empirical quantum chemical calculations were used to explore the sites of protonation. Heat of formation diagrams of the matrix-analyte complexes were examined as a function of their configuration. Investigation of the optimized geometries allowed the location of bifurcated and linear hydrogen bonds between the non-polar analyte (e.g., Gly-Gly) and matrix molecules. In addition to these intermolecular bonds, in the case of His-His an intramolecular hydrogen bond was also formed within the analyte molecule. Proton affinity values were calculated for every dipeptide while the site of protonation was varied. The results seemed to indicate that for every dipeptide the amino terminus was more susceptible to protonation than the peptide bond. Due to increased stabilization effects in homo-oligomers (Gly_n), increasing the number of residues led to an increase in proton affinity. For basic dipeptides (e.g., His-His), the side chains had the highest proton affinity, underlining their role in MALDI of proteins.

Matrix-assisted laser desorption/ionization (MALDI) is effectively used for molecular mass determination of large biopolymers.^{1,2} In this method, a pulsed laser is used to irradiate the mixture of sample and matrix. Interaction of the laser beam with the mixture ejects both matrix and analyte molecules into the gas phase. The matrix molecules may undergo extensive fragmentation and ionization. Only a small portion of the biomolecules, however, become ionized and subsequently analyzed by the mass spectrometer.

The low ion yield in general, and the variable ionization efficiency in particular, are two important limiting factors in the application of MALDI. Proteins are known to show much stronger response than, for example, carbohydrates or most of the synthetic polymers. Even among similar size proteins there are great differences in the ionization yield. Bovine albumin or cytochrome *c*, for example, provide ample ion intensities, whereas no analyte specific ions can be observed at the same concentrations of pepsin or collagen. In mixtures of proteins certain components can dominate the spectra independent of relative concentrations. The presence of these components may diminish the response from other proteins bordering on complete suppression of the signal in extreme cases. These severe interferences hamper the applications of MALDI and make quantitation especially challenging.

Since the advent of MALDI, there have been several efforts directed toward the understanding of ion formation mechanisms in the laser desorption process.^{3–8}

The primary sources of ions are believed to be protonation, alkylation, and adduct formation. Protonated ions are formed by proton transfer from the matrix to the neutral analyte molecule either in the gas or in the solid phase. Attachment of hard-to-get-rid-of impurities, such as K or Na, results in alkalinized ions probably as a result of efficient ion/molecule reactions in the gas phase.³ Finally, adduct ions are formed through the attachment of the matrix ions or one of its fragments to the analyte species. The matrix is thought to play an essential role in the ionization process in the form of matrix photoionization in the initial ionization step, and in a variety of charge transfer mechanisms later.^{3,9} In both positive-ion mode, ion/molecule reactions have been proposed as analyte ionization mechanism by several groups.^{7,10}

In order to examine the origin of the differences in ion yield, we plan to eliminate some of the complexities involved in the desorption of proteins. A systematic study of natural proteins probing the role of residue composition would have limited scope because of their predetermined amino acid composition. Also, the large size of most of these proteins lead to added complications due to their secondary and tertiary structure. An ionization site buried inside the protein molecule may be much less accessible than the one exhibited on the surface. Therefore, we use short peptides of systematically varied composition to explore the role of amino acid residues in the MALDI process.

Another important factor in determining ion yield is the incorporation of the analyte molecules into the matrix. Peptides and proteins of different character may have different tendency to embed into matrix

* Author for correspondence.

materials. In the polar environment of matrix crystals, hydrophilic peptides may be easier to accommodate than peptides with hydrophobic side chains. Assuming that incorporation is a necessary requirement for successful ion formation, a correlation can be established between ion yield and hydrophobicity.

Gas phase basicities and proton affinities of non-volatile materials such as proteins and peptides have been studied extensively.¹¹⁻¹⁴ Recently, the effect of amino acid composition and chain length was probed using tandem (MS/MS) and Fourier transform (FT) mass spectrometric methods by two groups. Wu and Fenselau¹¹ and Sperling and Cassady¹² showed that the proton affinity of short peptides increases with increasing number of residues. Gas-phase cation affinities of regular and modified amino acids were investigated by Burllet and Gaskell.¹³ It was suggested that the amide bond might be competing with the N-terminal amino group at the protonation site. Moreover, Morgan and Bursey demonstrated that basic residues, such as Arg, Lys, and His, have the ability to direct protons toward their side chains.¹⁴ According to their conclusions in the absence of basic residues protonation takes place on the peptide bond. Gorman and Amster measured the gas-phase basicity of a series of peptides containing valine using MALDI.¹⁵ Their results suggest that the basicity of a dipeptide is nearly equal to the basicity of its most basic residue. Furthermore, they found indications of intramolecular hydrogen bonding between the amide carbonyl oxygen and the N-terminus nitrogen of valine containing dipeptides.

Protonation at the amino terminus as the sole source of ions in MALDI was ruled out, however, in experiments with cyclic peptides.¹⁶ Cyclic analogues of the melanocyte stimulating hormone core were analyzed by MALDI at 266 nm (frequency quadrupled Nd-YAG laser) using nicotinic acid matrix. Both protonated and radical cations of the cyclic peptides were observed.

Theoretical calculations can provide important insight into the possible locations of protonation. For the quantum chemical description of proton transfer and hydrogen bonding special treatment is required, because of the comparatively small bond energies involved and of the relatively low mass of proton. In the large systems of our interest *ab initio* calculations were not feasible. An appropriate semi-empirical molecular orbital method (AM1) had been introduced by Dewar and co-workers for the study of chemical reactions.¹⁷ Other semi-empirical methods, including MNDO, gave unrealistic repulsive energies for hydrogen bonded structures.¹⁸ These problems were overcome in AM1 by modifying the core repulsion function. Dannenberg and Vinson have successfully used AM1 for the study of hydrogen bonding in the hydration of protonated diamines¹⁹ and crystalline nitroanilines.²⁰ AM1 based potential energy surfaces were used to describe proton transfer in protonated water clusters by the Marcus theory.²¹ Recently, Stewart used an optimization algorithm to reparametrize MNDO resulting in the PM3 code.²² Although the empirical parameters are different for AM1 and PM3, similar results have been produced by both methods in terms of proton affinities and heats of formation.²³ In this work we used AM1 calculations to differentiate between likely and unlikely protonation sites in the matrix-analyte interactions.

Although a number of studies in the literature

attempted to identify the ionization processes in MALDI,^{6-7, 24-25} little attention was devoted to the significance of amino acid composition. Our work focused on exploring: (i) ion formation through proton transfer to specific amino acid residues in small peptides, (ii) the possible locations of protonation in the peptide, and (iii) the effect of wavelength on ion formation. We examined small di- and tripeptides composed of selected residues containing basic, aromatic, and neutral side chains.

EXPERIMENTAL

Instrumentation

A linear time-of-flight mass spectrometer (TOF 101, Comstock Inc., Oak Ridge, TN, USA) was modified to accommodate two laser ports, a viewport, and high accelerating voltage up to 30 kV. The pressure was consistently lower than 10^{-8} mbar in the ion source region. Above the probe tip, the 1 cm accelerating region was followed by a large diameter ion lens (\varnothing 7.13 cm) to maximize transmission. The interlocking design of lens elements eliminated field penetration and provided excellent field homogeneity. At the end of the 215 cm flight path the ions were detected by a two-stage microchannel plate assembly, biased to -1800 V. Due to the relatively low mass of analyte ions, the accelerating voltage was kept at 10.00 kV throughout this study. Two high stability power supplies (Series 205B, Bertan Associates, Inc., Hicksville, NY, USA) provided ripple-free operation even during high ion current operation.

The system was equipped with two laser sources: a nitrogen laser (VSL-337ND, Laser Science Inc., Newton, MA, USA) emitting at 337 nm wavelength, and a dye laser (LPD 3000, Lambda Physik, Goettingen, Germany) pumped at 308 nm by XeCl filled excimer laser (Lextra 50, Lambda Physik, Goettingen, Germany). The doubled output of the dye laser (Coumarin 540A dye) was tunable in 275–290 nm range. A fast photodiode was used to measure the pulse width and monitor the proper operation of the lasers. Pulse energies were recorded by a pyroelectric joule meter. The nitrogen laser delivered up to 110 μ J in 5 ns full width at half maximum (FWHM) pulses with maximum 5% shot-to-shot intensity fluctuations. Fluctuations in the average of 128 shots, however, were only around 1.4%. Thus, changes in fluctuations of the average intensity may carry information about the desorption process. The output of the doubled dye laser exceeded 400 μ J with 12 ns pulse width, when properly tuned. The laser irradiance was adjusted by a variable attenuator (935-5-OPT, Newport Corp., Fountain Valley, CA, USA) and focused by a 254 mm focal length quartz lens onto the sample probe at 45°. The schematic view of the instrument is shown in Fig. 1.

A 10 \times fast preamplifier (Model 9305, EG&G ORTEC, Oak Ridge, TN, USA) was followed by a variable-gain amplifier module to extend the dynamic range of detection. After the two amplification stages the ion current was recorded by a fast transient digitizer (TR8828D, LeCroy, Albuquerque, NM, USA). Data acquisition and analysis was performed on a 486D/33 MHz personal computer running custom made soft-

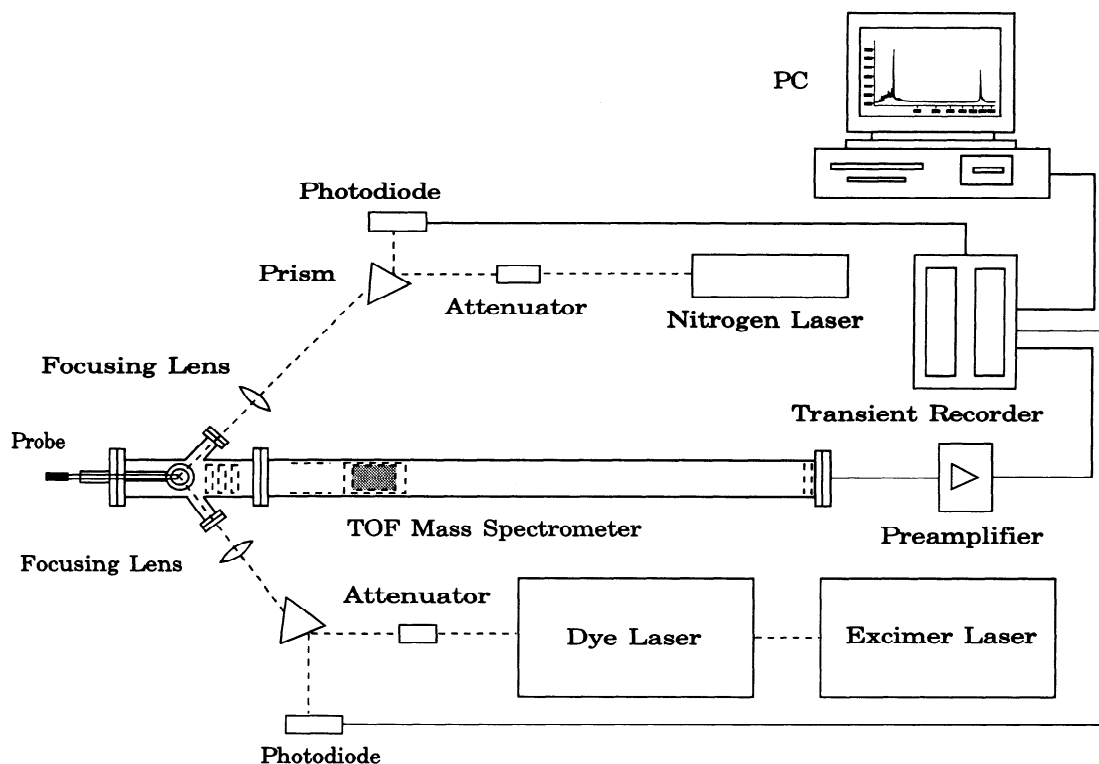


Figure 1. Schematic view of the time-of-flight mass spectrometer with variable wavelength laser ion source.

ware (TOFWARE, Ilys Software, Pittsburgh, PA, USA).

To provide uniform ionization conditions we kept the critical instrumental parameters—accelerating voltage, laser irradiance, detector bias—constant throughout the investigation. The laser irradiance was set to somewhat above the threshold for the poorest responding analyte and this value was kept constant for all the samples.

Sample preparation

The experiments were conducted using 3,5-dimethoxy-4-hydroxy-cinnamic acid (sinapinic acid, SA, Aldrich, Milwaukee, WI, USA) and 2,5-dihydroxybenzoic acid (DHB, Sigma, St. Louis, MO, USA) as matrices. We had to recrystallize the DHB twice in order to remove the excessive amount of sodium salts present in the original product. Matrix solutions were prepared fresh every day in 7:3 (v/v) HPLC grade acetonitrile deionized water mixture. The analytes were purchased from Sigma (Sigma, St. Louis, MO, USA), with the exception of His-His, Gly-Gly-Gly, and Ala-Ala (Nutritional Biochemicals Corporation, Cleveland, OH, USA), Gly-Ser California Foundation for Biochemical Research, Los Angeles, CA, USA) and *N*-methylacetamide (Aldrich, Milwaukee, WI, USA). Stock solutions of the peptides were prepared in 0.1% trifluoroacetic acid (TFA) to obtain 5×10^{-4} M concentrations. In the experiments, 2 μ L aliquot of the analyte was mixed with 10 μ L of matrix solution on the probe tip (diameter 5 mm) leading to higher than 1000 matrix-to-analyte ratio. To test the effect of premixing control experiments were performed after vortex mixing in microcentrifuge tubes. The spontaneous mixing of matrix and analyte during the drying process and vortex premixing led to identical results. A stream of cold air

was used to remove the solvent and produce an even distribution of crystals on the probe tip.

Data acquisition and analysis

To ensure representative sampling and minimize the distortions of statistical analysis a data acquisition protocol was developed. Spectra were collected from five randomly selected spots on the probe tip. At each spot 100 consecutive spectra were recorded for further analysis. From this set only spectra with overloaded or missing matrix peaks were discarded. The percentage of rejected shots never exceeded 5%. From the remaining data 50 consecutive spectra were averaged to eliminate shot-to-shot variations and improve signal-to-noise ratio. The statistical analysis was performed on five of these data sets for every peptide.

For the comparison of shot-to-shot variations in Gly-Gly and His-His, the 50 consecutive spectra were also analyzed without averaging. In order to calculate accurate peak area and peak height values for both analyte and matrix ions, the raw time dependent ion current data was saved in ASCII format, and analyzed by a scientific graphics package (Origin, MicroCal Software, Inc., Northampton, MA, USA). After accurate baseline corrections, the peak parameters were calculated and subjected to statistical analysis.

METHODS OF CALCULATION

All geometry optimization and energy calculations were carried out using the AM1 method as implemented in the MOPAC 6.0 package.²⁶ The code was run on a 100 MHz, R4000 workstation (IRIS Indigo XZ4000, Silicon Graphics, Mountain View, CA, USA). Equilibrium configurations and dynamics reaction paths were visualized by the XMOL package (Version 1.3.1, Research Equipment Inc.).

The initial geometries of several analytes (*N*-methylacetamide, Gly-Gly, His-His, Gly-Ser, Lys-Lys, Arg-Lys, Ala-Ala, and Gly-Gly-Gly) and the matrix (sinapinic acid) were optimized separately. Since peptide bonds joining the amino acid residues are planar, the nitrogen bonds, unlike in their normal pyramidal structure, are also coplanar. Semi-empirical methods have a tendency to underestimate the energy barrier between flat and pyramidal nitrogen. Therefore, corrections were introduced to increase the HNCO energy barrier (58.58 kJ/mol for *N*-methylacetamide.²⁶ Geometries were defined in terms of internal coordinates and optimized for every configuration using Pulay's force field method.²⁷ For the optimization of the matrix-analyte complexes, the hydroxy of the carboxylic group on the matrix was directed toward the site of protonation.

Single and multiple hydrogen bond formation between the matrix and analyte was examined at the peptide bond, the amino endgroup, and the heteroatom on the side chains of basic peptides. In order to locate bifurcated, inter-, and intramolecular hydrogen bonds, optimized geometry heavy atom distances were traced for every suspected binding site within the separated analytes and in complexes with the matrix.

To study the energetics of hydrogen bonding, the sum of matrix and analyte heats of formation were compared to the heat of formation value obtained for the combined matrix-analyte system. The difference was attributed to heat of formation of the hydrogen bond(s) formed between the two molecules. In every configuration the entire analyte molecule was moved toward the matrix and heat of formation diagrams were plotted as a function of the heavy atom distance between the proton donor group of the matrix and the electronegative atom in the analyte. The presence and position of a minimum in the diagram was indicative of hydrogen bond formation between the two species. The analyte-matrix complexes were investigated starting from several initial configurations for the comparison of possible hydrogen bonding sites.

To obtain proton affinity values, heats of formation were calculated separately for the isolated peptide molecules in their neutral form. Subsequently, various sites on each molecule were protonated and the corresponding heat of formation values were determined. The proton affinities were computed using the equation $PA(A) = \Delta H_f(A) + \Delta H_f(H^+) - \Delta H_f(AH^+)$, where *A* is the peptide of interest and $\Delta H_f(H^+) = 1536.2$ kJ/mol.^{28, 29}

Condensed phase proton transfer is governed by a double minimum potential energy surface between the proton acceptor and donor species.³⁰⁻³¹ A double well structure facilitates protonation by providing localized states in the vicinity of both molecules.³² Proton transfer rates can be estimated by using the height of the enthalpy of formation barrier, the distance between the minima, and the energy of the proton in the transition complex. Our proton tunneling rate calculations have been presented elsewhere.³³ It is known that the transition state energy barriers are severely overestimated by the AM1 approximation, for it neglects the long-range *d* and *f* orbitals. Accurate barrier heights can be obtained from *ab initio* studies, but the size of peptide-matrix systems leads to prohibitive computation times. For quantitative description of

these activation energy barriers, the Marcus theory has been proposed in combination with semi-empirical methods.²¹ Results for simple peptide-matrix systems will be presented in a separate publication.

Since it had been suggested that the acid-base properties of excited molecules were responsible for analyte protonation in MALDI,⁶ our investigations also covered the excited states of certain complexes. In accordance with the Franck-Condon principle,³⁴ all excited state calculations were performed assuming that the geometries of the excited species were the same as their optimized ground state configurations.

RESULTS AND DISCUSSION

Sites and efficiency of protonation in MALDI

The three possible localized sites of protonation in a simple peptide are the amino terminus, the carbonyl oxygen in the peptide bond, and certain side chains. In addition, there are several delocalized proton sharing options discussed in detail in the Literature.^{11, 30-31} These multicenter states seem to be more favored in the case of longer peptide chains.¹¹⁻¹² Since the present study deals with di- and tripeptides, here we only consider the three localized configurations.

In order to separate the contribution of protonation at a single isolated peptide bond we investigated *N*-methylacetamide, CH₃CONHCH₃, the simplest molecule exhibiting the CONH feature. We tried to obtain MALDI spectrum of *N*-methylacetamide using several matrices, and a large variety of irradiation conditions. No evidence of analyte related ions was observed. These negative results indicated that in short peptides the isolated peptide bond was not the likely site of protonation under MALDI conditions. In the presence of endgroups and in the case of longer peptides, however, one can not exclude the participation of peptide bonds in accommodating the proton.

To probe the role of endgroups and side chains in the protonation process, a series of di- and tripeptides were investigated. Table 1 summarizes the relative and absolute intensities for the MH⁺ ions at 337 nm excitation. The appearance of the MH⁺ species for

Table 1. Absolute and relative MH⁺ molecular ion intensities obtained using nitrogen laser excitation for different di- and tripeptides

Compound	Character of side chain	Relative intensity ^a	Absolute intensity ^b
<i>N</i> -methylacetamide	N/A	0.00 ± 0.00	0.00 ± 0.00
Gly-Gly	np-np ^c	0.08 ± 0.04	3.60 ± 2.09
Ala-Ala	np-np	0.17 ± 0.06	4.60 ± 2.69
Gly-Ser	np-p	0.17 ± 0.03	5.69 ± 0.77
Lys-Lys	b-b	0.06 ± 0.02	3.61 ± 0.92
His-Lys	b-b	0.19 ± 0.05	7.34 ± 3.05
His-His	b-b	0.44 ± 0.08	21.1 ± 1.9
Arg-Lys	b-b	0.47 ± 0.07	26.0 ± 4.5
Gly-Gly-Gly	np-np-np	0.23 ± 0.05	10.9 ± 2.6
Gly-His-Gly	np-b-npo	0.30 ± 0.09	11.5 ± 5.2

^a Relative intensity is the ratio of protonated analyte and matrix ion intensities.

^b Absolute intensity refers to the protonated analyte intensity in arbitrary units.

^c The abbreviations used in the table are: b = basic, np = nonpolar, p = polar, N/A = not applicable.

Gly-Gly, Ala-Ala, and Gly-Gly-Gly confirms that MALDI, like other soft ionization methods, may lead to protonated amino terminus. Gly-Gly, however, is at the bottom of both the relative and the absolute ion intensity scale for peptides, indicating that the amino terminus itself or in combination with one peptide bond has relatively weak affinity to protons. We detected about three times higher ion yields for the longer peptide chain (i.e., Gly-Gly-Gly), pointing to the possible role of differences in proton affinities.¹¹ This effect may be explained by intramolecular proton delocalization between the amino terminus and the two peptide bonds.

Basic side chains are known to provide added opportunities for proton attachment. There is an ongoing debate about the order of gas-phase basicities of the basic residues.¹³ Recent kinetic measurements seem to support the idea that the liquid phase order, Arg > Lys > His changes to Arg > His > Lys in a gas-phase environment.¹³ Our MALDI experiments with four basic dipeptides (Arg-Lys, His-His, His-Lys, Lys-Lys) demonstrated strong enhancement in production yields over Gly-Gly with the exception of Lys-Lys. Lys-Lys showed very similar behavior to Gly-Gly, indicating a profound departure from Lys being the second most basic residue in liquid phase ($pK = 10.0$). The effect of other basic residues (Arg, His) was a dramatic improvement (>5 times) in absolute MALDI intensities accompanied by similar improvement in intensity ratios relative to the matrix signal (see Table 1). The general order of MH^+ abundances followed the Arg > His > Lys rule if we assumed that the most basic residue defined the basicity of the dipeptide. Thus, the observed MH^+ intensity order for dipeptides Arg-Lys > His-His > His-Lys > Lys-Lys is coherent with the established gas phase basicity scale.¹³ Remarkably, His-His showed higher protonation yields than His-Lys pointing to the compounding effect of basicities. The role of the most basic residue is expected to become less important in the case of longer polypeptide chains due to limited access to buried residues in globular conformations. In addition, marked differences in matrix embedding are likely for globular proteins exhibiting polar and non-polar surfaces.

The presence of one or two Lys residues in little or no enhancement over the Gly-Gly case. In other words, the $-(CH_2)_4-NH_2$ side chain of Lys behaved almost exactly like the amino terminus of the peptide. The additional 'amino terminus' due to Lys did not increase the chances of protonation in MALDI of dipeptides. This also points to the necessary interplay between the $-NH_2$ group and the carbonyl oxygen of the peptide bond in accommodating the proton.

Zoomed MALDI time-of-flight spectra of the molecular ion region of dipeptides Gly-Gly and His-His are compared in Fig. 2. The presented spectra display 10 single shot responses in SA matrix to demonstrate shot-to-shot variations (see below). Strong matrix peaks at m/z 225 ($M'H^+$) and m/z 207 ($M' - 17^+$) were accompanied by protonated dipeptide signal at m/z 133 (Gly-Gly H^+) and at m/z 293 (His-His H^+). The basic dipeptide showed ion intensities comparable to matrix ion intensities. In the case of Gly-Gly much weaker Gly-Gly H^+ related signal was observed (Fig. 2(a)) together with poorer signal-to-noise ratio.

Two additional dipeptides, Ala-Ala with non-polar

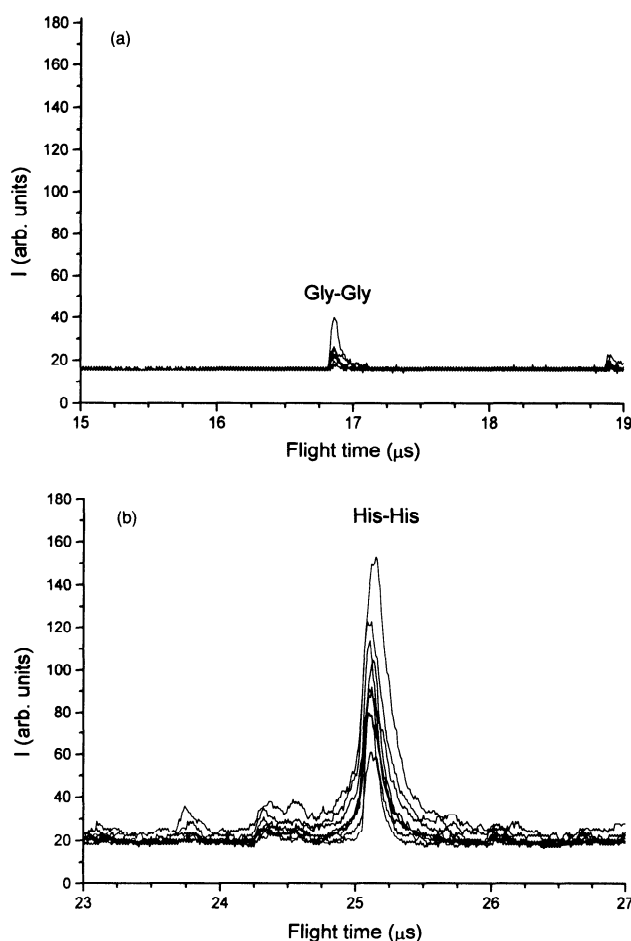


Figure 2. Superimposed traces in multiple-shot positive-ion MALDI mass spectra of (a) Gly-Gly and (b) His-His in sinapinic acid matrix (10 shots). Laser: nitrogen (337 nm).

side chains and Gly-Ser with a hydroxyl containing side chain, showed significant enhancement over Gly-Gly ion yields. The relatively high yields in Ala-Ala could be explained by the electron releasing nature of the methyl group. Increasing the partial negative charge on other groups ($-NH_2$, peptide bond) the presence of the methyl group may have led to increased protonation. The polar side chain in Gly-Ser is a known source of additional hydrogen bond formation between matrix and analyte. The extra hydrogen bond can open a new channel for the proton transfer reaction. Combined enhancement due to the extension of chain length and the effect of a basic residue was observed in the case of Gly-His-Gly leading to ion intensities in the Gly-His-Gly > Gly-Gly-Gly > His-Lys order.

Although less often than in electrospray ionization, multiply charged ions are known to appear in MALDI. It was interesting to note that no doubly charge peptide ions appeared under any set of experimental parameters. The lack of higher charge states in the spectra was probably due to the relatively small size of our analytes leading to very unfavorable energy states for even doubly charged species.

Shot-to-shot and average reproducibility

The significant shot-to-shot variation of ion current displayed in Fig. 2 is one of the shortcomings of the

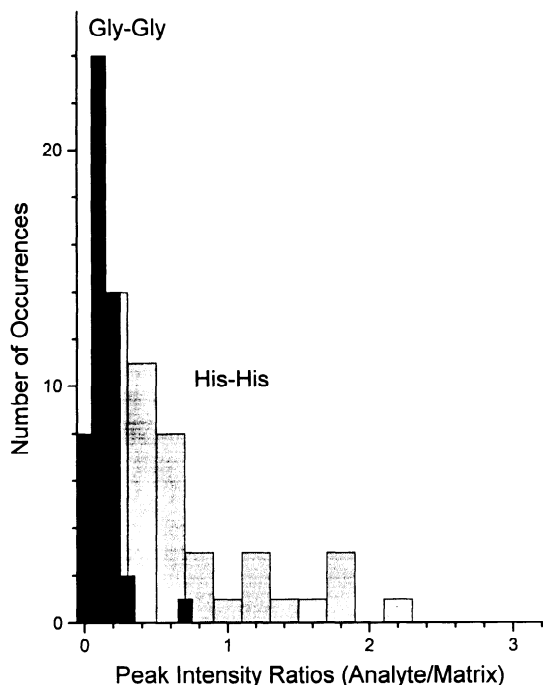


Figure 3. Shot-to-shot variations of peak intensity ratios for dipeptides of different character (Gly-Gly: np-np, His-His: b-b). Matrix: sinapinic acid. Laser: nitrogen (337 nm).

MALDI method. It hinders the comparison of spectra from different samples and ultimately plagues quantification. There are several known sources of signal instability in the MALDI process. Laser fluence and directional fluctuations are probably among the most important factors. Since the ion yield around the threshold varies with the 5th power of laser irradiance, ~15% fluence variation leads to about 100% variation in ion current.

The wide range of ion yields generated by 50 single shots is demonstrated for Gly-Gly and His-His in Fig. 3. Very different occurrence statistics of relative peak intensities were observed for the non-polar (e.g., Gly-Gly) and basic (e.g., His-His) dipeptides. In the non-polar case the distribution bordered on zero and up to 16% of laser pulses did not result in analyte ion formation. For His-His there was always analyte response, but the fluctuations were still quite substantial.

Comparing the statistics on the averages gives a somewhat different picture. Table 1 shows that the relative standard deviations for 50-shot averages are ~50% for Gly-Gly and ~18% for His-His. Similar differences cannot be explained away by the relatively small fluctuations in average laser fluence (2–3%). Since the 50-shot averages have been collected at different locations on the sample surface, it is conceivable that these fluctuations have more to do with variations in sample composition, coverage, or embedding. Indeed, embedding non-polar or hydrophobic peptides into crystals of polar molecules led to higher energy chemical defects than did incorporating particles of similar nature to the crystals. Although incorporation of both Gly-Gly and His-His into SA results in unfavorable defects, the related excess energy may in part be compensated by polar host-guest interactions in the case of His-His.

Wavelength studies

Three of the 20 amino acid residues show significant absorption in the near-ultraviolet region. The relevant absorption maxima in aqueous solutions are at 280 nm ($\epsilon_{280} = 5600 \text{ M}^{-1} \text{ cm}^{-1}$) for Trp, at 275 nm ($\epsilon_{275} = 1230 \text{ M}^{-1} \text{ cm}^{-1}$) for Tyr, and at 267 nm with lower molar absorptivity for Phe.³⁵ None of these chromophores, however, present appreciable absorption at the nitrogen laser wavelength, 337 nm. Thus, by changing the wavelength to the absorption maximum of the strongest absorber (280 nm) within the accessible range of our instrument, we hoped to observe the effect of energy deposition into the analyte.

We compared the MALDI mass spectra of five short peptides containing one of the chromophore amino acid residues at 337 nm and at 280 nm laser wavelength. In all five cases, profoundly more complex spectra were observed at shorter wavelength irradiation. The nitrogen laser excitation resulted only in protonated molecules, whereas the 280 nm dye laser excitation led to significant fragmentation. An example is shown in Fig. 4, where the response of Trp-Gly is depicted at the two different wavelengths. The protonated molecule was the only analyte ion at 337 nm, whereas three fragment ions were generated along with $[M + H]^+$ at 280 nm. It was remarkable that the strongest analyte related ion was the tryptophan side chain fragment, R_1^+ . Also abundant was the immonium ion, A_1 , probably resulting from fragmentation initiated by the energized R_1 side chain. Weak ion signal corresponded to OH loss from the protonated molecule.

Similar fragmentation schemes were observed for the other four peptides as well. The major fragments are listed in Table 2. As a general trend, the formation of a radical cation from the energized side chain was detected. In many cases the A_n and Z_n fragments were more abundant than the Y_n series, a remarkable departure from fast-atom bombardment and chemical ionization fragmentation patterns. We attributed this difference to the energizing role of the chromophore. The bond breakages leading to A_n and Z_n fragments most of the time happened next to the aromatic side chain. These fragmentation patterns show strong similarity to

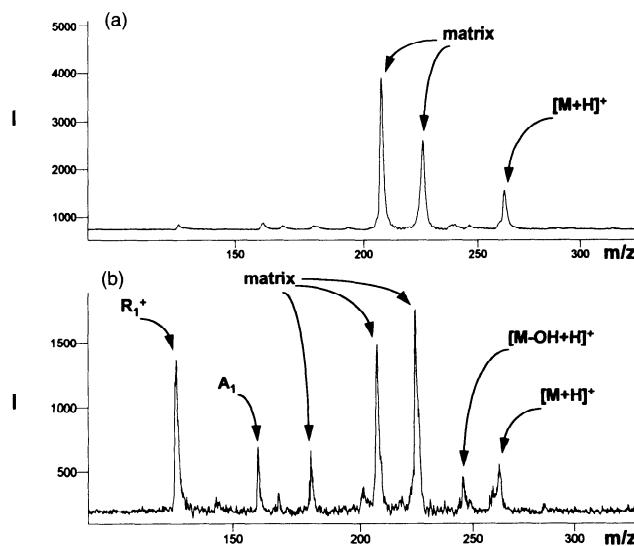


Figure 4. Comparison of MALDI spectra at (a) 337 nm and (b) 280 nm for Trp-Gly in SA matrix.

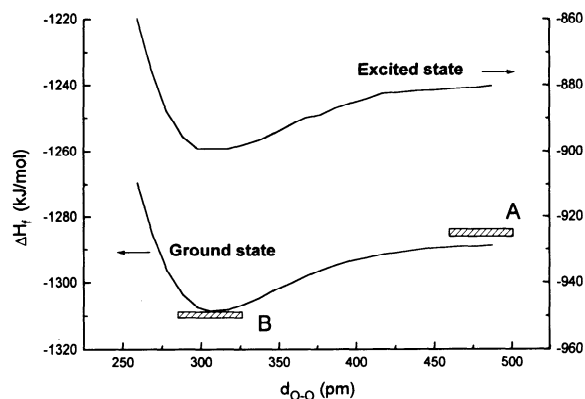


Figure 5. Ground and excited state hydrogen bond formation between the carbonyl oxygen in the peptide bond of Gly-Gly and carboxylic hydrogen in SA. A: compounded heat of formation of the individual molecules, B: complex heat of formation.

diagram indicated the length of the hydrogen bond between the two species. The enthalpy of formation diagrams in the ground and excited states of Gly-Gly and SA are presented in Fig. 5. The heat of formation at the minimum corresponds to the heat of formation value obtained for the hydrogen bonded system. As the distance between the two heavy atoms increases, the hydrogen bond detaches and the heat of formation becomes equal to the compounded heat of formation of the two molecules. The position of the minimum at 310 pm shows the calculated hydrogen bond length in reasonable agreement with the measured 272 pm.³⁴ When multiple hydrogen bonds are present, breaking one hydrogen bond does not disrupt the matrix-analyte structure. In these cases the final heat of formation includes the contribution of the remaining hydrogen bond(s). The presence of these multiple hydrogen bonds may facilitate the incorporation of peptides into the host crystal.

The energetics of the intermolecular hydrogen bonds were also studied. For this purpose compounded heats of formation of matrix and analyte were compared to that of the complex. The stabilization of the complex can be attributed to the presence of hydrogen bonds. Heat of formation of the hydrogen bonds in complexes are presented in Table 3. These calculated heat of formation values are within the measured range of -6.28 to -31.4 kJ/mol.³⁴ Some of these values (e.g. the hydrogen bond formed at the amino terminus of Gly-Gly and SA) seem to correspond to a single hydrogen bond, while others are related to multiple hydrogen bond formation. As discussed previously in the experi-

Table 3. Heats of formation corresponding to hydrogen bonds between analyte and matrix in different configurations.

Compound	Investigated site	ΔH_f (kJ/mol)	Number of H bonds and type
Gly-Gly + SA	Peptide bond	-2.6	1s + 1b ^a
	Amino group	-6.06	1s
Gly-Ser + SA	Peptide bond	-25.1	1s + 1b
	Side chain	-30.5	2s
	Amino group	-17.3	1s
His-His + SA	Side chain	-22.6	2s

^as: single; b: bifurcated.

Table 4. Comparison of calculated proton affinities^a, PA_{calc} , for selected dipeptides protonated at different sites with experimental values, PA_{exp}

Compound	Site of protonation	PA_{calc} (kJ/mol)	PA_{exp} (kJ/mol)
Gly-Gly	Amino endgroup	860.65	916.71 ^b , 905.00 ^c
	Peptide bond	839.69	
Gly-Gly-Gly	Amino endgroup	870.15	933.45 ^b
	Peptide bond	866.26	
	Peptide bond	878.56	
Lys-Lys	Amino endgroup	888.43	
	Peptide bond	855.55	
	Side chain (1) ^d	891.99	
	Side chain (2) ^d	963.91	
His-His	Amino endgroup	963.70	
	Peptide bond	948.39	
	Side chain	1001.0	
Gly-Ser	Amino endgroup	874.16	910.44 ^c
	Peptide bond	851.99	
	Side chain	811.7	
Arg-Lys	Amino endgroup	888.22	
	Peptide bond	876.93	
	Side chain (1)	896.30	
	Side chain (2)	907.89	
	Side chain (2)	1032.28	

^a Proton affinity; $PA(A) = \Delta H_f(A) + \Delta H_f(H^+) - \Delta H_f(AH^+)$.

^b From Ref. 11.

^c From Ref. 37.

^d (1) refers to the side chain close to the C-terminus and (2) to the side chain close to the N-terminus.

mental results, *N*-methylacetamide with an isolated peptide bond gave no molecular ion peak in MALDI. From the experimental results, it seems that some of the preformed protonation sites such as the peptide bond of Gly-Gly contribute less to the protonation than others. In general, no correlation can be found between calculated heats of formation for hydrogen bonds and measured MH^+ intensities. This observation points to the role of gas-phase processes in MALDI ion formation.

In order to assess the driving force of the protonation process, proton affinity values were calculated for six peptides. The following protonation sites were considered (i) the carbonyl oxygen in the peptide bonds (ii) the nitrogen in the amino terminus of all peptides, and (iii) the electronegative atom in the side chains of Gly-Ser, His-His, Lys-Lys, and Arg-Lys. The heats of the formation of the neutral isolated molecules were computed. For every peptide, the heat of formation of the protonated molecule was also calculated with the proton placed at different sites. The proton affinities were expressed using the equation explained in the Methods of Calculation section. Results of these calculations are presented in Table 4. Calculated proton affinities are compared to experimental values when available. For all the selected peptides, except Gly-Ser and Gly-Gly-Gly, the proton affinity value was lowest when protonation occurred at the peptide bond. In peptides with non-basic side chains such as Gly-Gly and Gly-Ser, the calculated proton affinity values are highest at the amino endgroup, confirming the earlier studies which showed that the amino terminus is the preferred protonation site in these dipeptides.³⁷

Comparison of proton affinities with the available experimental data show consistently lower calculated values (Table 3). This discrepancy may be related to the neglecting of *d* and *f* orbitals in the AM1 code.

As has been shown by experiment, increasing the number of glycine residues in a homo-oligomer leads to increase in the proton affinity.¹¹ Our calculated values also show an increase in proton affinity from Gly-Gly to Gly-Gly-Gly. This increase can be explained by charge-induced dipole interaction, intramolecular hydrogen bonding, internal solvation of proton or statistical effects.¹¹

Dipeptides containing basic residues show greatly increased proton affinities at their side chains. The highest calculated proton affinity was observed at the side chain of Arg in Arg-Lys. This corresponds to earlier findings indicating that arginine is the most basic amino acid and has the highest proton affinity in the gas phase.¹³ Among the three heteroatoms in the Arg side chain the nitrogen which is connected with a double bond to the last carbon of the side chain has the highest proton affinity due to the possibility of charge delocalization. His-His showed a higher proton affinity at the side chain than all of the investigated protonation sites in other peptides, except for Arg-Lys. These results are consistent with our experimental results and with the known gas-phase basicity scale.¹³ Lysine is known to be the third basic amino acid residue. The proton affinity values obtained for Lys-Lys at the peptide bond, amino terminus, and the side chain close to the C-terminus are not significantly higher than other non-basic dipeptides. The side chain close to the N-terminus has a relatively higher calculated proton affinity and seems to be responsible for the protonation of the molecule. In the MALDI spectra of Lys-Lys the ion yield obtained was much less than His-His, suggesting that although Lys-Lys is basic protonation does not occur to the expected extent. This may be the result of intramolecular hydrogen bonding observed in the calculations.

Arg-Lys and His-His with high proton affinities produce the strongest protonated molecular ion peaks in their MALDI spectra (Table 1). On the other hand, Gly-Gly and Gly-Ser with non-basic side chains give significantly lower ion yields, with the preferred site of protonation being the amino terminus. These findings are in good correlation with our experimental results and point to the importance of amino acid composition in MALDI of proteins. Polypeptides with a higher number of basic amino acid residues are expected to produce stronger protonated molecule peaks. Although other factors such as the conformation of the protein are important, the amino acid composition seems to play a significant role in the MALDI ion yield of proteins.

Acknowledgements

Financial support from the National Science Foundation (Grant No. CTS-9212389) was used to purchase the excimer laser and part of the dye laser system. In-kind contribution from the George Washington University made it possible to acquire the second harmonic generator and laser coupling optics. The authors were also supported in part by the George Washington University Facilitating Fund. Some of the peptide samples were kindly provided by Dr W. E. Schmidt of the George Washington University.

REFERENCES

1. M. Karas and F. Hillenkamp, *Anal. Chem.* **60**, 2299 (1988).
2. F. Hillenkamp, M. Karas, R. C. Beavis and B. T. Chait, *Anal. Chem.* **63**, 1193A (1991).
3. H. Ehring, M. Karas and F. Hillenkamp, *Org. Mass Spectrom.* **27**, 472 (1992).
4. R. C. Beavis, *Org. Mass Spectrom.* **27**, 864 (1992).
5. A. Westman, P. Demirev, T. Huth-Fehre, J. Bielawski and B. U. R. Sundqvist, *Int. J. Mass Spectrom. Ion Processes* **130**, 107 (1994).
6. M. E. Gimon, L. M. Preston, T. Solouki, M. A. White D. H. Russell, *Org. Mass Spectrom.* **27**, 827 (1992).
7. A. Vertes and R. Gijbels, in *Laser Ionization Mass Analysis*, A. Vertes, R. Gijbels and F. Adams (Eds), John Wiley, New York 1993, pp. 127-175.
8. P. Liao and J. Allison, *J. Mass Spectrom.* **30**, 408 (1995).
9. C. D. Mowry and M. V. Johnston, *Rapid Commun. Mass Spectrom.* **7**, 569 (1993).
10. S. K. Viswanadham, D. Hercules, E. M. Schreiber, R. R. Weller and C. S. Giam, *Anal. Chem.* **60**, 2346 (1988).
11. Z. Wu and C. J. Fenselau, *J. Am. Soc. Mass Spectrom.* **3**, 863 (1992).
12. B. Sperling and C. Cassady, *Proceedings of the 40th Annual Conference on Mass Spectrometry and Allied Topics, Washington, DC, ASMS, Santa Fe*, pp. 172-173.
13. O. Burllet and S. J. Gaskell, *J. Am. Soc. Mass Spectrom.* **4**, 461 (1993).
14. D. G. Morgan and M. M. Bursey, *Org. Mass Spectrom.* **29**, 354 (1994).
15. G. S. Gorman and I. J. Amster, *J. Am. Chem. Soc.* **115**, 5729 (1993).
16. A. Vertes, L. Balazs and R. Gijbels, *Rapid Commun. Mass Spectrom.* **4**, 263 (1990).
17. M. J. S. Dewar, E. G. Zoebisch, E. F. Healy and J. J. Stewart, *Am. Chem. Soc.* **107**, 3902 (1985).
18. M. J. S. Dewar and D. M. Storch, *J. Am. Chem. Soc.* **107**, 3898 (1985).
19. J. J. Dannenberg and L. K. Vinson, *J. Phys. Chem.* **92**, 5635 (1988).
20. L. K. Vinson and J. J. Dannenberg, *J. Am. Chem. Soc.* **111**, 2777 (1989).
21. J. Y. Choi, E. R. Davidson and I. Lee, *J. Comput. Chem.* **10**, 163 (1988).
22. J. J. P. Stewart, *J. Comp. Chem.* **10**, 209 (1989).
23. S. Schroder, V. Dagget and P. Koolman, *J. Am. Chem. Soc.* **113**, 8922 (1991).
24. A. Vertes, G. Irinyi and R. Gijbels, *Anal. Chem.* **65**, 2389 (1993).
25. A. Vertes, R. Gijbels and R. Levine, *Rapid Commun. Mass Spectrom.* **4**, 228 (1990).
26. MOPAC: M. B. Coolidge, J. J. P. Stewart and J. Frank, Seiler Research Laboratory, United States Air Force Academy, CO 80840 (1990).
27. P. L. Cummings and J. E. Geady, *J. Comp. Chem.* **10**, 939 (1989).
28. R. A. J. O'Hair, S. Gronert and T. D. Williams, *Org. Mass Spectrom.* **29**, 151 (1994).
29. T. L. Brown, H. E. LeMay Jr. and B. E. Bursten, *Chemistry: The Central Science*, 6th Edn, Prentice-Hall, New Jersey 1994, pp. 1012-1015.
30. P. P. Schmidt, *J. Phys. Chem.* **97**, 4249 (1993).
31. S. Scheiner and L. Wang, *J. Am. Chem. Soc.* **114**, 3650 (1992).
32. L. D. Landau and E. M. Lifshitz, *Quantum Mechanics*, Pergamon Press, New York 1977, pp. 164-185.
33. A. Vertes, *Proceedings of the 42nd Annual Conference on Mass Spectrometry and Allied Topics, Chicago, IL, ASMS, East Lansing 1994*, p. 2.
34. S. Vinogradov and R. Linnell, *Hydrogen Bonding*, Van Nostrand, New York 1971, pp.83-113.
35. E. A. Permyakov, *Luminescent Spectroscopy of Proteins*, CRC Press, Boca Raton 1993, pp. 35-56.
36. D. M. Lubman, in *Laser Ionization Mass Analysis*, A. Vertes, R. Gijbels and F. Adams (Eds), John Wiley, New York 1993, pp. 321-368.
37. J. W. McKierman, C. E. A. Beltrame and C. Cassady, *J. Am. Soc. Mass Spectrom.* **5**, 718 (1994).